Supporting Information

For

Energetic Basis for Inhibition of Calcium Phosphate Biomineralization by Osteopontin

Meng Li,[†] Lijun Wang,[*,†] and Christine V. Putnis[‡,§]

[†]College of Resources and Environment, Huazhong Agricultural University, Wuhan 430070, China

[‡]Institut für Mineralogie, University of Münster, 48149 Münster, Germany

[§]Department of Chemistry, Curtin University, Perth, Western Australia 6845, Australia

SI APPENDIX

1. SI Materials and Methods

1.1. KPFM for surface potential measurements

1.2. AFM imaging and nucleation rate measurements

1.3. Tip decoration and force spectroscopy measurement

1.4. Single-molecule force spectroscopy analysis

SI APPENDIX REFERENCES

SI APPENDIX TABLE (S1)

SI APPENDIX FIGURES (S1-S11)

1. SI Materials and Methods

1.1 KPFM for Surface Potential Measurements. Surface potential measurements of preparing mica-supported mixed lipid membranes, individual lipid constituents on mica, and bare mica were performed by amplitude modulated Kelvin probe force microscopy (AM-KPFM) using a Nanoscope V- Multimode 8 AFM (Bruker, Santa Barbara, CA) with a conductive AFM tip (MESP, Bruker). A two-pass procedure was employed where the surface topography was generated by standard tapping mode with a pixel density of 256 × 256 in the first pass, and the surface potential was measured with a lift height of 30 nm above the surface. In the second pass, the tapping drive piezo was turned off and an oscillating alternating current voltage $V_{AC}\sin(\omega t)$ (ω is the resonant frequency of the cantilever) was applied directly to the tip. The surface potential was determined by adjusting the V_{DC} on the tip until the oscillation amplitude went to zero and the surface potential was the same as the tip voltage (V_{tip}),[1] which can be given by,

$$V_{tip} = V_{AC}\sin(\omega t) + V_{DC} \quad [S1]$$

The voltage applied to the tip was recorded by the Nanoscope V controller to map a voltage image of the surface. The surface potential measurements were performed at least at three different locations for each sample. A gold surface (PFKPFM-SMPL, Bruker) with a function of about 5.10 eV was used as a reference to calibrate the work

function of the tips before and after each surface potential measurement.[2] The data were analyzed with the Nanoscope Analysis 1.50 software (Bruker).

1.2. AFM Imaging and Nucleation Rate Measurements. All *in situ* heterogeneous nucleation experiments were conducted by collecting time-lapse images of calcium phosphate nuclei that formed on the substrate as a function of time using a Nanoscope V- Multimode 8 AFM (Bruker, Santa Barbara, CA) in ScanAsyst mode. AFM images were collected using commercial silicon nitride probes (Bruker, tip mode ScanAsyst-fluid$^+$, k = 0.7 N/m and tip radius < 12 nm, Santa Barbara, CA) with scan rates of 2-3 Hz. The chosen ScanAsyst mode was used in our experiments on account of the forces arising from the interactions between the AFM tip and the forming Ca-P nuclei. To acquire relatively high resolution images, some parameters were manually adjusted, including ScanAsyst noise threshold, low pass deflection bandwidth, and Peak Force Amplitude.

A high-precision syringe pump (Razel Scientific Instruments model R100-E) was used to continuously pump the supersaturated solutions into the flow cell at a constant rate of 10 mL/h at 25 ^{o}C to ensure steady-state conditions, which reduced diffusion-limited conditions for Ca-P nucleation and maintained the reactant solutions in the cell for a sufficiently long residence time to nucleation on the substrate. The steady-state nucleation rates were shortly determined after the onset of Ca-P precipitation, and the number of nuclei increased linearly with time, typically within

the first 1-2 hours of each experiment. For each experiment, three independent replications were performed.

As shown in Fig. 1, the 2:1:1 POPC/SM/DChol monolayer exhibited two different domains: liquid-ordered (LO) phase (SM/DChol) and liquid-expanded (LE) phase (single-component of POPC phase).[3] The LO phase showed a very regular and densely packed structure surrounded by a LE phase. In contrast to the LO phase, the surface potential of the LE phase was of slightly negative charge (Fig. S5), and the area of LE phases were much larger than that of LO phases in our experiments. Thus we only counted the particles nucleated on the surface of the LE phase. As well, in order to accurately estimate the nucleation rate (in units of nuclei per m^2 per second), we made two assumptions:

i. Each AFM observed nucleus was developed from a single Ca-P cluster, i.e., each nucleus overcame a free-energy barrier to achieve a critical size of a Posner's cluster which could be detected by an AFM tip, but it was not necessarily the thermodynamically most stable. Therefore, we only counted the particles in heights that were larger than 0.8 nm.

ii. Due to the initial formation of nuclei mixed with lipid agglomerates within minutes, we just counted all subsequently formed nuclei on the LE phase.

1.3. Tip Decoration and Force Spectroscopy Measurement. Force-distance curve based AFM imaging was performed using functionalized triangular microlever with Si_3N_4 tips (Bruker, tip model SNL-10, CA) and lever D (nominal spring constant,

k = 0.06 N m^{-1} and tip radius = 2 nm). According to reported procedures,[4] tip functionalization was carried out as follows. First, bare tips were treated under UV/ozone for 10 min, followed by immerion in acetone for 40 min, rinsed in ethanol, then dried under a nitrogen stream. Cleaned tips were coated with gold using an ion sputtering instrument (model JFC-1600, JEOL, Japan) and rinsed again in acetone and ethanol. The coated tips were then immersed in a solution of N, N-dimethylformamide (DMF) (Sigma, St. Louis, Missouri) containing 0.2 mM of heterobifunctional cross-linker LC-SPDP for 40 min. The LC-SPDP reagent is a unique group of sulfhydryl- and amine-reactive heterobifunctional crosslinker, where the sulfhydryl-reactive portion with a pyridyl disulfide can adsorb to gold and the amine-reactive portion with a *N*-hydroxysuccinimide (NHS) ester can react with the N-terminal amine or lysine resides of peptide to from an amide bond. The unbound cross-linker was removed by rinsing in DMF, followed by ethanol. The tips were immersed in phosphate buffer saline (PBS) solution with 100 nM OPN peptides for 12 hours. Functionalized tips were rinsed in ultrapure water prior to use to remove the nonspecifically bound peptides and avoid the salt deposit.

Force spectroscopy measurements between modified tips and the HAP (100) surface were performed in a liquid cell filled with freshly prepared PBS solution. At the beginning of experiments, the inverse optical lever sensitivity (InvOLS) of the functionalized cantilever were detected via the laser deflection method[5] that determines the slope of the piezo travel distance vs. the change in photodiode voltage

when the cantilever tip was in contact with the surface. Then, the spring constant was calibrated with the thermal noise method[6] by fitting a harmonic oscillator to the thermal noise spectrum. A spot with a relatively smooth surface was chosen in the force-distance curve-based AFM imaging. To account for surface heterogeneities, a custom routine was applied to randomly move the AFM tip on the HAP surface to give a representative average. Affected by the drifting, contamination and coating damage of the cantilever,[7] the cantilever InvOLS can change during the experiment. Thus, we calibrated the InvOLS of the cantilever before and after recording force-distance curves. The rational variations of the cantilever InvOLS of about 5-8 % within several hours were accepted.[7] Measurements were obtained by approaching the peptide functionalized tip to the HAP (100) surface with a constant approach velocity of 200 nm s^{-1} until it was in contact with the substrate (a deflection trigger of 2-3 nm and a dwell time for 1 second before pulling away), and retracting the tip at seven various pulling speeds of 20 nm/s, 200 nm/s, 601 nm/s, 1.04 μm/s, 1.90 μm/s, 2.6 μm/s to 3.91 μm/s. In our experiments, a total of 256 individual extension-retraction cycles were recorded for each pulling rate. Three independent measurements were done for each condition.

1.4. Single-Molecule Force Spectroscopy Analyses. The InvOLS and spring constant were calibrated and averaged at the beginning and at the end of the experiment to calculate the force-distance curves. Typically, online NanoScope analysis software can automatically convert the raw deflection signal (volts) into force

signal by multiplying voltage signal to the InvOLS and the spring constant. Peptides that connected the AFM tip represented a non-linear spring. The actual nominal loading rate can never be the same as the nominal loading rate applied by the cantilever.

To properly depict the complicated extension of peptide, a nonlinear least-square fitting method of the worm-like chain (WLC) model was used to analyze the number of tethers being stretched,[8] and the relation between the entropy force (F) and the extension of the peptide (x) can be written as follows:

$$F=\frac{k_bT}{L_p}\left(\frac{1}{4}\left(1-\frac{x}{L_c}\right)^{-2}+\frac{x}{L_c}-\frac{1}{4}\right) \quad [S2]$$

where k_b is the Boltzmann's constant, T is temperature, L_p and L_c are the apparent persistence and contour length of the peptide molecules obtained by fitting the peak before desorption. The resulting contour lengths were plotted in a frequency distribution and then fitted with a Gaussian distribution to define the distribution mode, and thus the most probable value was extracted (Fig. S9). In our experiments, the values of the contour length obtained by the Gaussian fitting correspond approximately to the theoretical value of (assumed) an average length of 0.35 nm per amino acid.[9] We noted that the distribution of contour length values exhibited a region that the contour length was larger than that of the monomer itself. We attributed it to the fact that several monomers may have bound together to the AFM tip and the ensemble was being stretched by the tip. If peptide alone had been covalently bound to both the tip and the HAP surface, we could determine whether these binding events

were specific using such analysis of the bond rupture in the force-separation trace. Thereby, every FD curve should be fitted by the WLC model (Fig. S10) to identify a specific interaction between the peptide and HAP surface.

Opposing to equilibrium binding affinities, the typical rupture force for a relatively weak biochemical bond is not constant but determined by the loading rate, $f \sim \ln r$, when it is driven far from equilibrium, where r can be replaced by the instantaneous loading rate from the slope of the force-time curve just prior to the rupture event, $r \sim \mathrm{d}f/\mathrm{d}t$.[10, 11] Because the time period (Δt) that a single-bond is out of contact with the crystal surface is very brief, thus r can be considered constant as is shown in Fig. 3C, $r = \Delta f/\Delta t$.

All measurements were performed with a very rigid piezoelectric scanner which stretched the peptides until the bond ruptured and AFM recorded the applied force in real time. Therefore, as the piezo scanner moved away from the HAP surface, a sudden jump where the transition from the bound state to the unbound state was defined as the measured rapture strength of the bond, although the biological bond would eventually be broken by thermal fluctuations for a long time (a period called the bond's natural lifetime) in the absence of load force.[12] As the loading rate was much smaller than the frequency of the thermal fluctuations, the external force was limited by the overall potential energy landscape of the system. Thus, there existed a minimal force to break the bond, which is an important point for the analysis of ΔG_{B}.[12, 13]

To accurately describe the nonlinear force spectra and extract the energetic and kinetic parameters, we used the analytical approximation methods developed by Friddle et al..[4, 13] Briefly, this method assumes that force spectroscopy passes through two primary regimes with a sufficiently wide range of loading rate: a near-equilibrium regime characterized by a finite force where the loading rate is sufficiently small, and a kinetic regime where rapture force is related to the loading rate. The two-state equation of probability of bound state $p_b(t)$ at time t can be given by:[4, 12, 13]

$$\frac{\mathrm{d}p_b}{\mathrm{d}t} = -k_u(t)p_b + k_b(t)p_u \qquad \text{[S3]}$$

where p_u is the probability of bound state at time t. k_u and k_b are the instantaneous kinetic unbinding and binding rate, respectively.[12, 13] We should note that it is impossible for us to observe a rupture force below the equilibrium force f_{eq}. Thus, when we transform the two-state equation from time to force dependence, we should integral the equation by starting at f_{eq} and simplify the Eq. S3 as,

$$\int_1^{p_b} \frac{\mathrm{d}p_b^{'}}{p_b^{'}} = -\frac{1}{r}\int_{f_{\mathrm{eq}}}^{f} k_u(f^{'})\,\mathrm{d}f^{'} \qquad \text{[S4]}$$

By solving the Eq. S4, based on previous analysis,[13] the mean work is given by

$$\langle W \rangle \approx -\Delta G_{\mathrm{bu}}\left(1 + \frac{k_b T}{x_{\mathrm{u}}\sqrt{2k\Delta G_{\mathrm{bu}}}}\exp[\psi X]\,\mathrm{E}_1[\psi X]\right)^2 \qquad \text{[S5]}$$

with $\psi = \exp[f_{\mathrm{eq}} x_{tr}/k_b T]$ and $X = \frac{k_1^0 k_{\mathrm{b}} T}{r x_{tr}}$

where k_1^0 is the intrinsic unbinding rate and x_{tr} is the distance between the free-energy minimum and transition state. Fitting Eq. S5 to the work data extracted the free-energy landscape of the peptide-HAP interaction.

SI References

SI References

1. Fujihira, M. Kelvin probe force microscopy of molecular surfaces. *Annu. Rev. Mater. Sci.* **1999**, *29*, 353-380.
2. Ma, J.; Cai, H. M.; He, C. W.; Zhang, W. J.; Wang, L. J. A hemicellulose-bound form of silicon inhibits cadmium ion uptake in rice (*Oryza sativa*) cells. *New Phytol.* **2015**, *206*, 1063-1074.
3. Benítez, I. O.; Talham, D. R. Calcium oxalate monohydrate precipitation at membrane lipid rafts. *J. Am. Chem. Soc.* **2005**, *127*, 2814-2815.
4. Friddle, R. W.; Battle, K.; Trubetskoy, V.; Tao, J. H.; Salter, E. A.; Moradian-Oldak, J.; De Yoreo, J. J.; Wierzbicki, A. Single-molecule determination of the face-specific adsorption of amelogenin's C-terminus on hydroxyapatite. *Angew. Chem., Int. Ed.* **2011**, *50*, 7541-7545.
5. Putman, C. A. J.; De Grooth, B. G.; Van Hulst, N. F.; Greve, J. A detailed analysis of the optical beam deflection technique for use in atomic force microscopy. *J. Appl. Phys.* **1992**, *72*, 6-12.
6. Hutter, J. L.; Bechhoefer, J. Calibration of atomic-force microscope tips. *Rev. Sci. Instrum.* **1993**, *64*, 1868-1873.
7. Pfreundschuh, M.; Martinez-Martin, D.; Mulvihill, E.; Wegmann, S.; Muller, D. J. Multiparametric high-resolution imaging of native proteins by force-distance curve–based AFM. *Nat. Protoc.* **2014**, *9*, 1113-1130

8. Bustamante, C.; Marko, J. F.; Siggia, E. D.; Smith, S. Entropic elasticity of λ-phage DNA. *Science* **1994**, *265*, 1599-1600.

9. Fantner, G. E.; Adams, J.; Turner, P.; Thurner, P. J.; Fisher, L. W.; Hansma, P. K. Nanoscale ion mediated networks in bone: osteopontin can repeatedly dissipate large amounts of energy. *Nano Lett.* **2007**, *7*, 2491-2498.

10. Bell, G. I. Models for the specific adhesion of cells to cells. *Science* **1978**, *200*, 618-627.

11. Evans, E.; Ritchie, K. Dynamic strength of molecular adhesion bonds. *Biophys. J.* **1997**, *72*, 1541.

12. Noy, A.; Friddle, R. W. Practical single molecule force spectroscopy: How to determine fundamental thermodynamic parameters of intermolecular bonds with an atomic force microscope. *Methods* **2013**, *60*, 142-150.

13. Friddle, R. W.; Noy, A.; De Yoreo, J. J. Interpreting the widespread nonlinear force spectra of intermolecular bonds. *Proc. Natl. Acad. Sci. U.S.A.* **2012**, *109*, 13573-13578.

14. Hoyer, J. R.; Asplin, J. R.; Otvos, L. Phosphorylated osteopontin peptides suppress crystallization by inhibiting the growth of calcium oxalate crystals. *Kidney Int.* **2001**, *60*, 77-82.

15. Talham, D. R.; Backov, R.; Benitez, I. O.; Sharbaugh, D. M.; Whipps, S.; Khan, S. R. Role of lipids in urinary stones: Studies of calcium oxalate precipitation at phospholipid monolayers. *Langmuir* **2006**, *22*, 2450-2456.

SI Table

Table S1. Values of B, ln(A), and γ are calculated from the heterogeneous surface nucleation on lipid raft membranes in supersaturated HAP solutions and ΔG_B is calculated from force spectroscopy measurements of OPN peptides adsorbed on the (100) face of HAP.

	B	ln(A)	γ (mJ m^{-2})	ΔG_B (kcal mol^{-1})
a	-130.3	25.5	75.7	–
b	-145.2	25.5	78.5	–
c	-414.9	26.2	111.4	-46.6
d	-234.9	25.9	92.1	-32.7
e	-1076.2	28.8	153.0	- 91.4
f	-713.5	27.0	133.4	-76.1

a: nucleation on mica surface in pure supersaturated solutions.
b-f: nucleation on lipid raft membranes in the (b) absence of OPN peptides and the presence of (c) peptide 62-85, (d) peptide 66-91, (e) peptide 93-106 and (f) peptide 99-115.

SI Figures

SNESHDHMDDMDDEDDDDHVDSQD	**62-85**
HDHMDDMDDEDDDDHVDSQDSIDSND	**66-91**
DDVDDTDDSHQSDE	**93-106**
DDSHQSDESHHSDESDE	**99-115**

Fig. S1. Sequences of the four pairs of peptide segments from 62 to115 of OPN[14] used for Ca-P nucleation and single-molecule force spectroscopy determination.

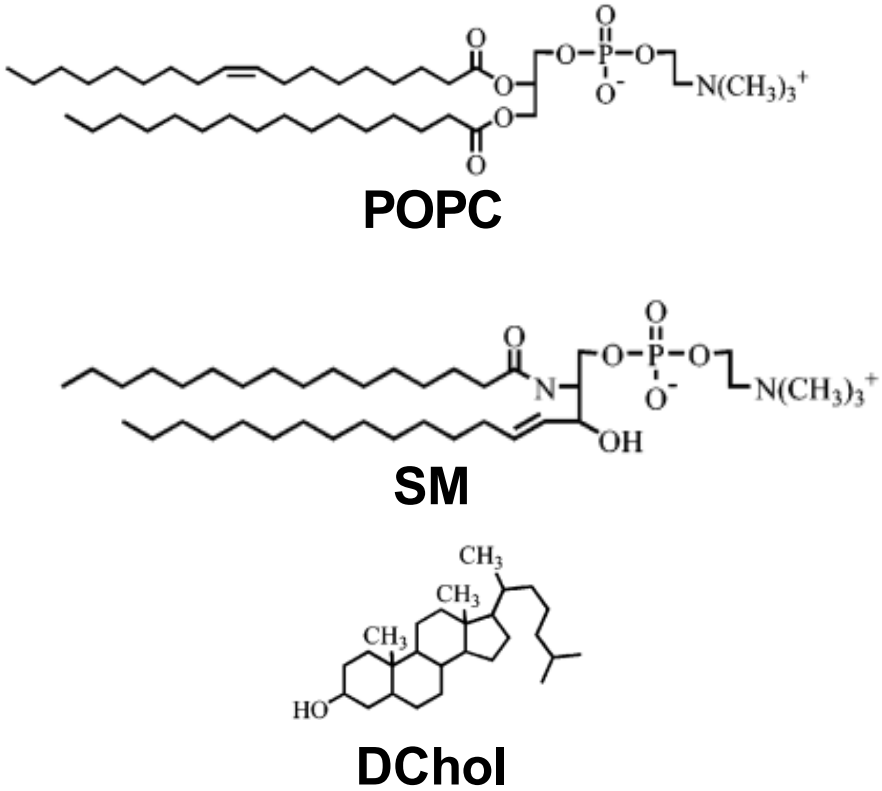

Fig. S2. Structures of the POPC, SM and DChol molecules.[15]

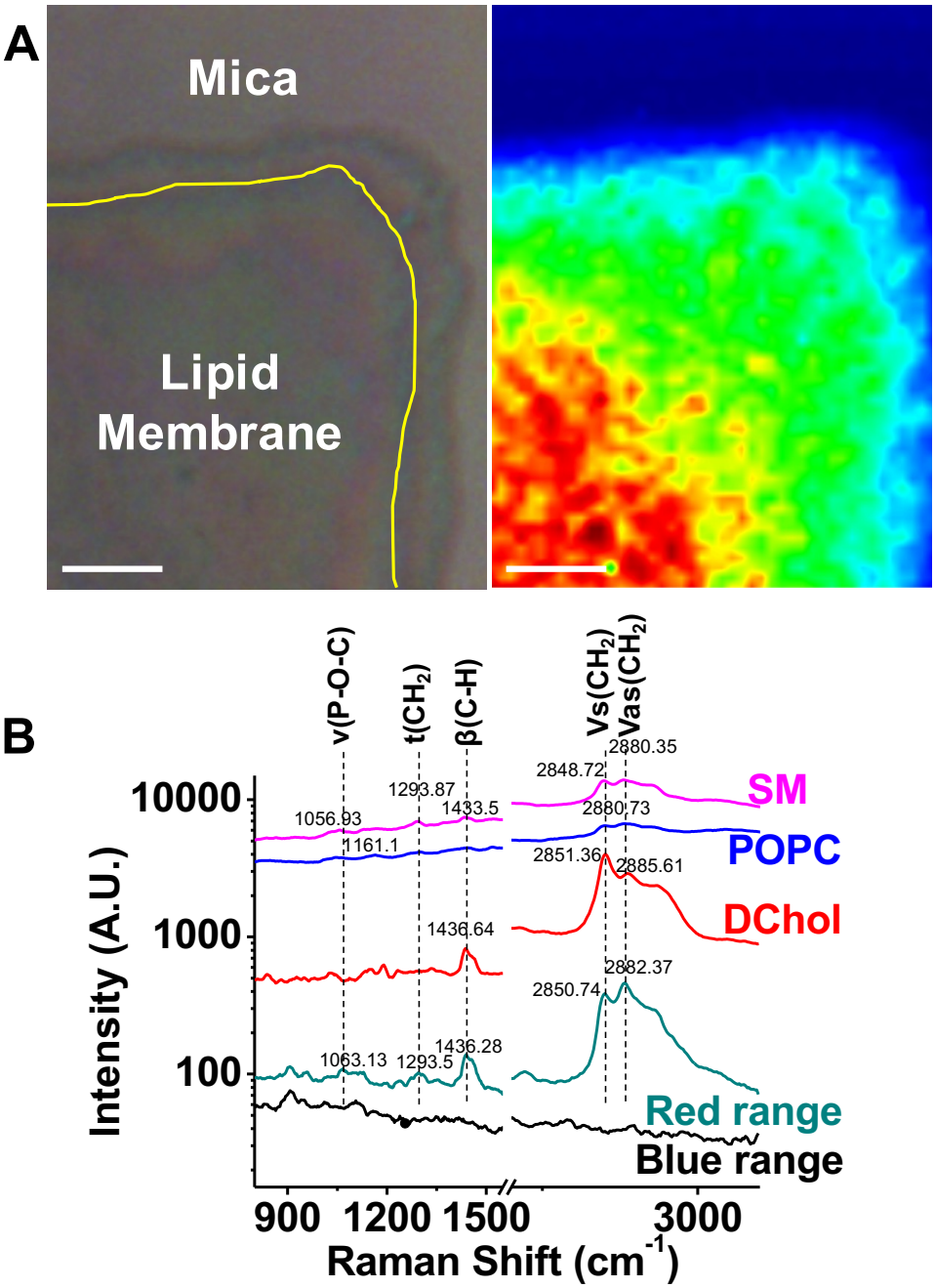

Fig. S3. (A) Micrograph (left) and Raman imaging (right) of the newly prepared lipid raft membrane with mixed three constituents on mica (scale bar: 4 μm). The curved yellow line (left micrograph) shows the boundary between mica and the coated lipid membrane. The color change from blue to red (right image) indicates an increase of

the peak intensity at 2790-3020 cm^{-1}, characteristic for lipids. (B) Raman spectra taken from blue and red areas in (A), and the standard SM, POPC or DChol.

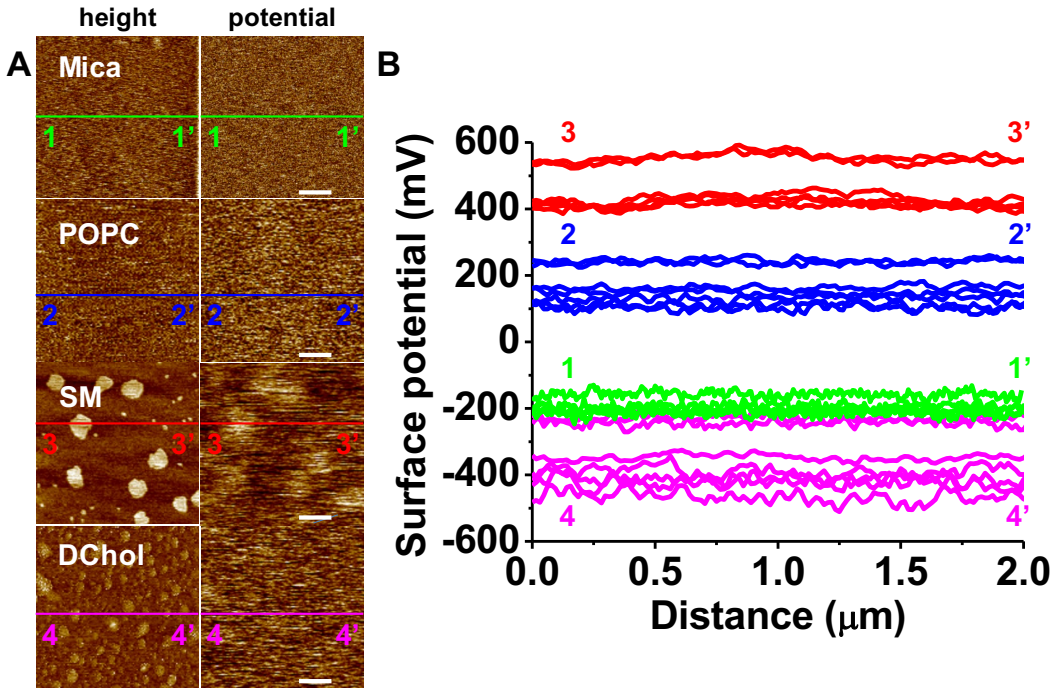

Fig. S4. Surface potential of the substrates of bare mica and standard reagents of POPC, SM or DChol coated on mica. (A) AFM height and surface potential images of bare mica and mica coated with POPC, SM or DChol (scale bar: 400 nm). (B) The surface potential profiles along lines 1→1', 2→2', 3→3', and 4→4' in (A).

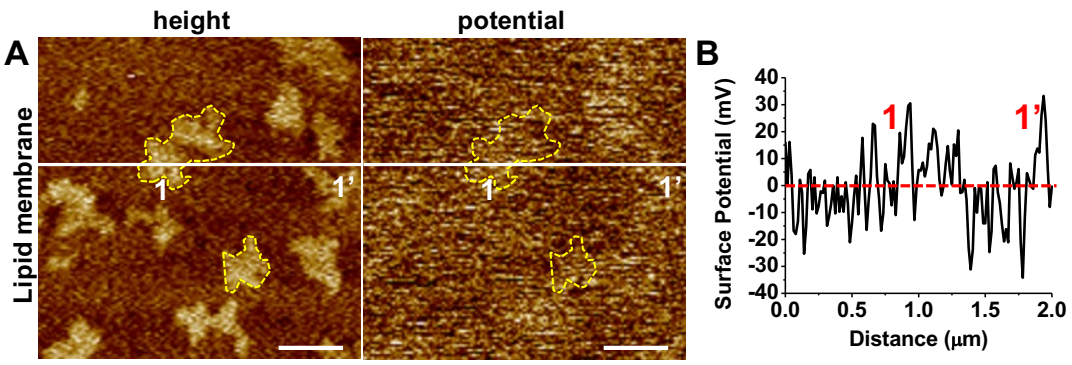

Fig. S5. (A) Representative AFM height and surface potential images of lipid raft membranes (scale bar: 400 nm). (B) The surface potential distribution along line 1→1' in (A) indicates a relatively positive charged surface in LO domains (10-30 mV) and a relatively negative charged surface in LE phases (-10- -30 mV). The average surface potential of LE domains is -33.5±19.3 mV (n = 12).

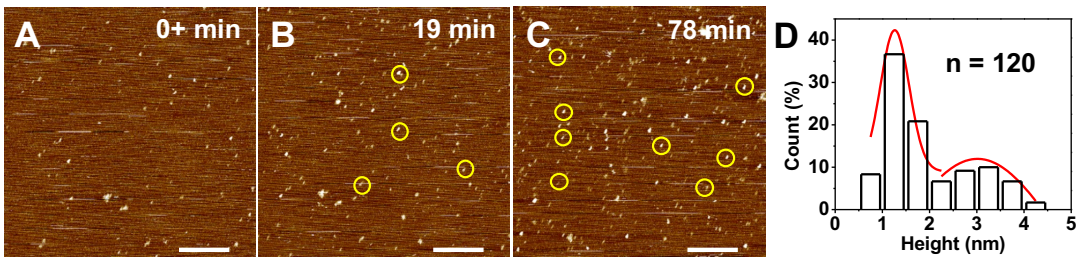

Fig. S6. (A-C) A time sequence of AFM height images showing *in situ* nucleation of Ca-P particles on lipid raft membranes at σ_{HAP} = 13.6 in the absence of OPN peptides (scale bar: 400 nm). (D) The corresponding height distribution of nucleated nanoparticles in (C) showing small and large nanoparticles with average heights of 1.4 ± 0.1 nm and 3.0 ± 0.1 nm, respectively.

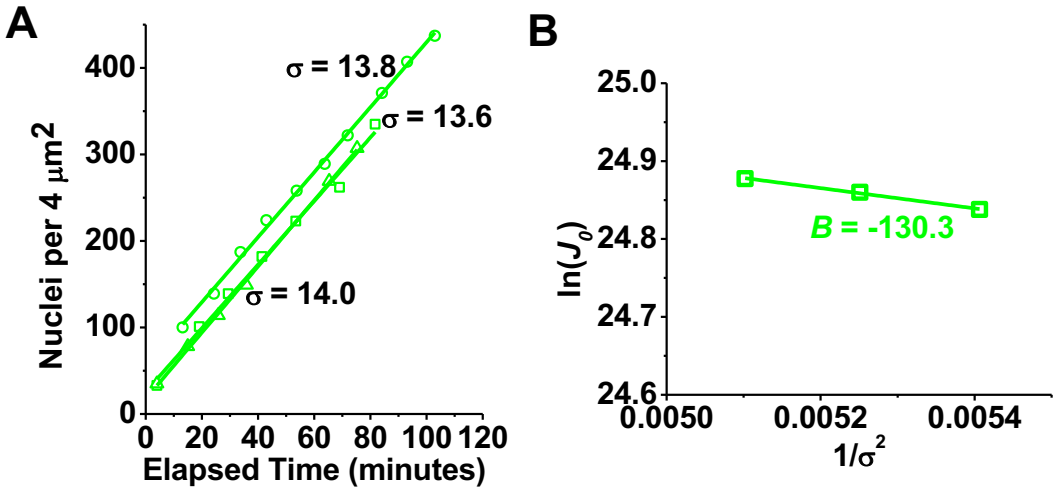

Fig. S7. (A) The dependence of nucleation events on a mica surface with time in different supersaturated solutions in the absence of OPN peptides. (B) Nucleation rate measurements follow the linear relationship predicted by Eq. 1. The slope *B* of -130.3 is smaller than that of -145.2 on mica coated by lipid membranes in pure supersaturated solutions.

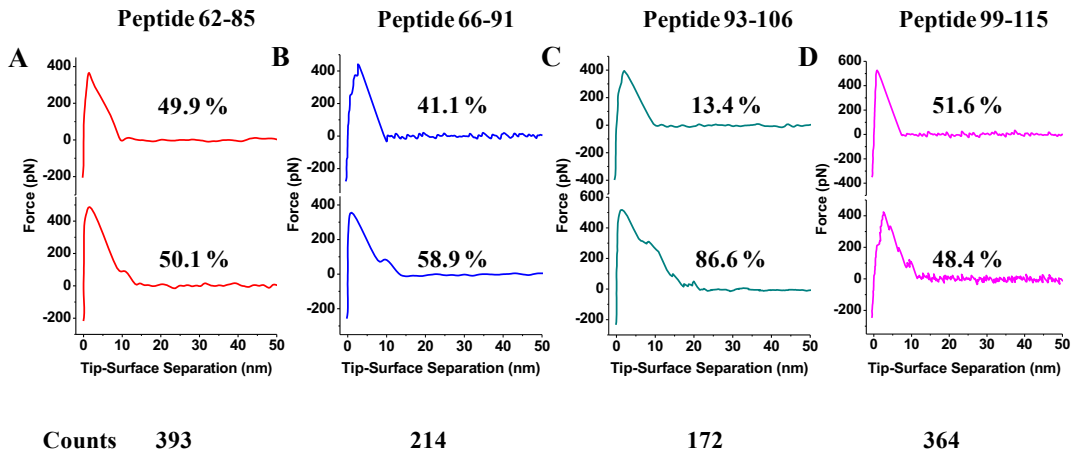

Fig. S8. Different FD curve shapes obtained from experimental pulling curves for (A) peptide 62-85, (B) peptide 66-91, (C) peptide 93-106, and (D) peptide 99-115, respectively. Two typical motives of single-bond forces (top) and flat plateau forces (bottom) were observed in the FD curves. The corresponding percentage of each motive is given. The number of observed events is 393, 214, 172 and 364 for peptide 62-85, 66-91, 93-106, and 99-115, respectively.

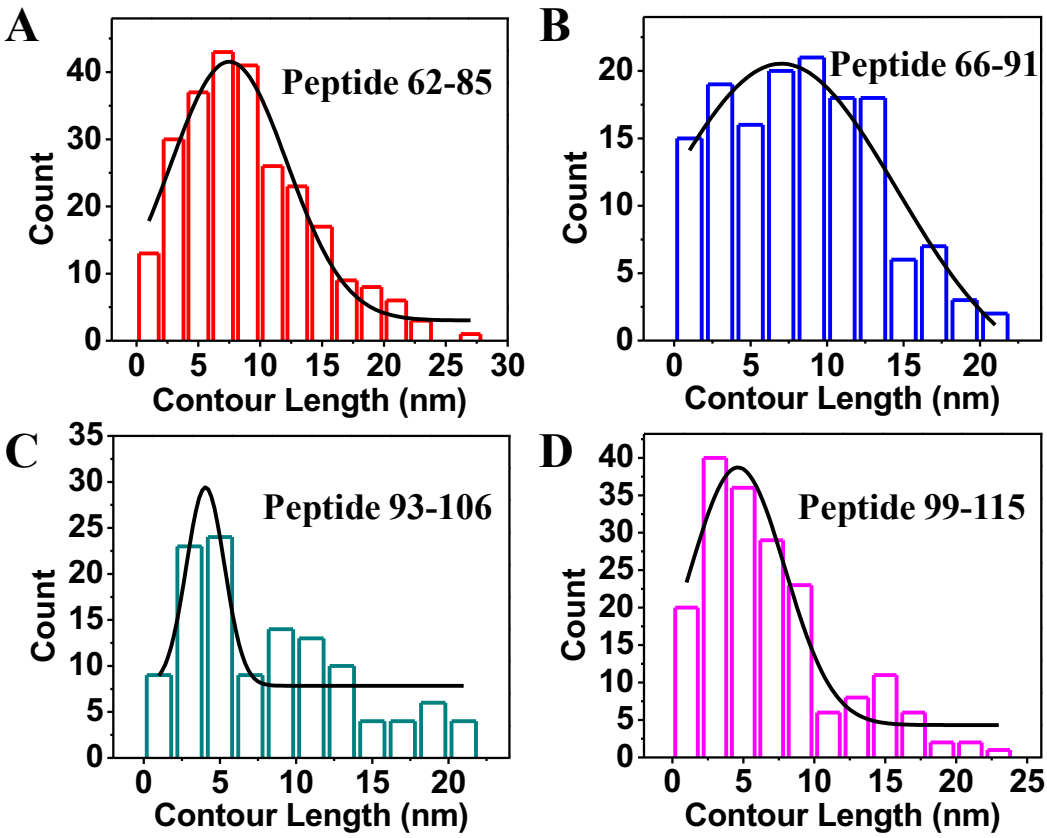

Fig. S9. Distributions of contour length values of (A) peptide 62-85, (B) peptide 66-91, (C) peptide 93-106, and (D) peptide 99-115 measured by FD curves and the most probable values are obtained by Gaussian fitting. The contour lengths of peptide 62-85, peptide 66-91, peptide 93-106 and peptide 99-115 are 7.5 ± 0.3, 7.0 ± 0.7, 4.0 ± 0.3, and 4.6 ± 0.4, respectively.

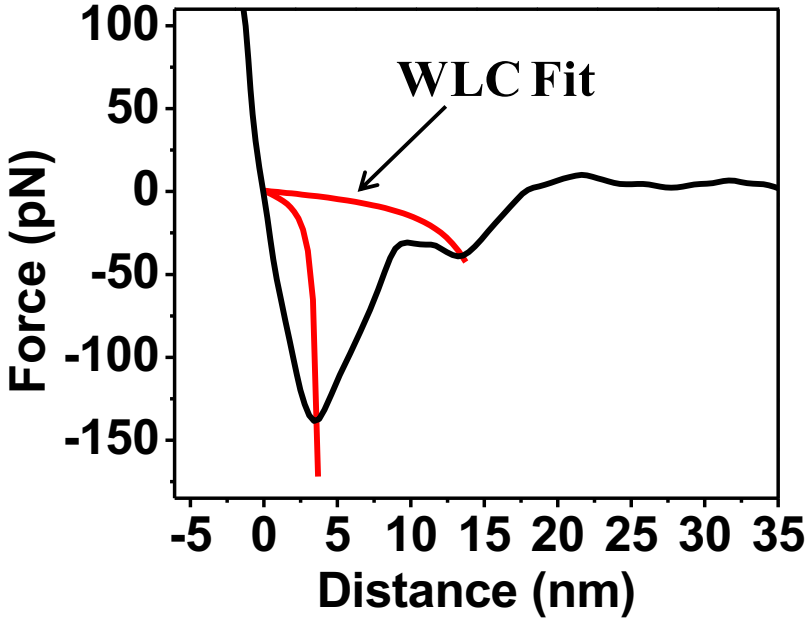

Fig. S10. WLC model fitting of the typical FD curve for pulling a single molecule of OPN peptide absorbed to the HAP (100) surface.

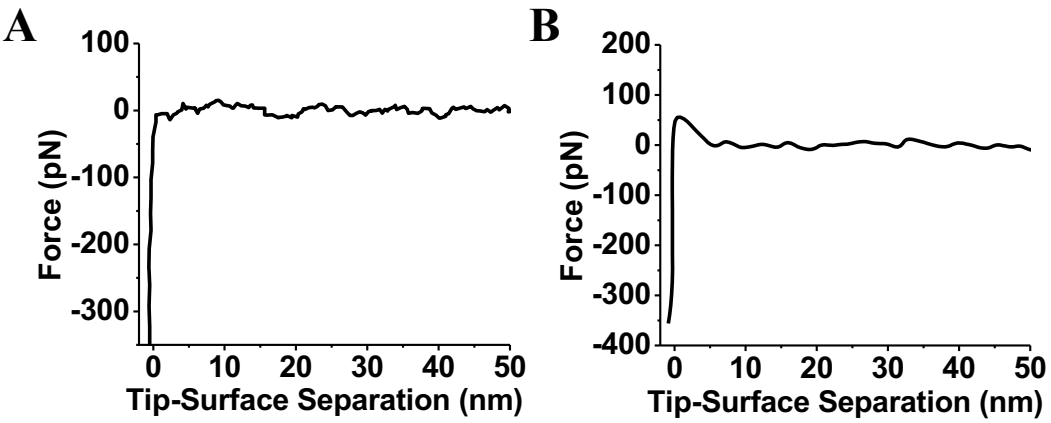

Fig. S11. Typical FD curves of the interaction of peptide 93-106 with lipid membranes show (A) no or (B) very small interaction between peptide 93-106 and lipid membrane rafts at a loading rate of 1.04 μm/s.